Synthesis and characterization of mesoporous alumina as a catalyst support for hydrodechlorination of 1,2-dichloropropane: effect of catalyst preparation method

Pil Kim[a], Younghun Kim[a], Changmook Kim[a], Heesoo Kim[a], Younggeun Park[a], Jae Ho Lee[a], In Kyu Song[b], and Jongheop Yi[a,*]

[a]*School of Chemical Engineering, Seoul National University, Shinlim-dong, Kwanak-ku, Seoul 151-742, Korea*
[b]*Department of Environmental and Applied Chemical Engineering Kangnung National University, Kangwondo 210-702, Korea*

Received 6 March 2003; accepted 6 June 2003

A mesoporous alumina was synthesized by a posthydrolysis method. The prepared mesoporous alumina was found to have randomly ordered pores, and retained relatively high surface area with narrow pore size distribution centered at ca. 4 nm. Nickel precursors were then supported on the mesoporous alumina by an impregnation (Ni-IMP) and vapor deposition (Ni-VD) method. Several characterizations were carried out in order to investigate physical and chemical properties of mesoporous alumina and supported Ni catalysts. TPR, XPS, and UV-DRS measurements revealed that the Ni-IMP catalyst retained much more amounts of surface nickel aluminate-like species than the Ni-VD sample. TPD experiments also showed that nickel aluminate species affected the adsorption amounts of reactant (1,2-dichloropropane). In the hydrodechlorination of 1,2-dichloropropane (DCPA), DCPA conversion over the Ni-VD catalyst was about two times higher than that over the Ni-IMP catalyst at 300 °C. It is probably due to the fact that the Ni-VD catalyst, which had low contents of nickel aluminate species compared to the Ni-IMP catalyst, exhibited higher degree of reduction than the Ni-IMP catalyst at pretreatment conditions. The difference in DCPA conversion between two catalysts was closely related to the degree of reduction of nickel species and the amounts of adsorption of DCPA onto the catalyst as well.

KEY WORDS: mesoporous γ-Al_2O_3; hydrodechlorination; 1,2-dichloropropane; Ni/γ-Al_2O_3; impregnation; vapor deposition; propylene.

1. Introduction

Since the discovery of ordered mesoporous silica with uniform pore size larger than 2 nm [1], many works have been reported for the synthesis of ordered mesoporous materials and the catalytic reactions using the related materials [2–6]. Mesoporous materials were not restricted to silica, and have also been reported for non-silica oxides [5–9], which found successful applications in the areas involving electron transfer, magnetic interaction, photocatalysis, and catalyst support.

Alumina has been widely used in catalysis as an inert support for active metals and as a part of bifunctional catalysts. Because of the importance of alumina as catalysts and supports, several attempts have been made to synthesize mesoporous alumina that can be applied to the catalytic reactions involving bulky molecules [9]. However, synthetic scheme for mesoporous silica was not directly applied to synthesize a mesoporous alumina, because the hydrolysis and condensation rate of aluminum precursor are much faster than those of silica precursor. Nonetheless, some researchers have reported that mesoporous alumina could be successfully synthesized by using a hydrolysis retarding agent [10] or posthydrolysis method [7]. Recently, a mesoporous alumina was successfully synthesized in this research group [7] by a posthydrolysis method at room temperature and at atmospheric pressure without using any hydrolysis retarding agents. It was revealed that the mesoporous alumina prepared in this nonhydrothermal synthesis method could be transformed into γ-form under mild conditions such as low calcination temperature.

In an environmental point of view, the catalytic hydrodechlorination of chlorinated organic compounds has an advantage over the conventional incineration process requiring harsh operation conditions and producing secondary pollutants. Besides, the catalytic process has an economic merit of producing useful hydrocarbons.

Hydrodechlorination of chlorinated alkanes over supported Ni catalysts has been widely studied by several researchers [11–15]. Recently, Choi *et al.* [13] reported that considerably high selectivity of propylene was obtained with Ni/SiO_2 in the hydrodechlorination of 1,2-dichloropropane. One research group [11,15] carried out the dehalogenation of cyclohexyl chloride over supported Ni catalysts. They reported that unsaturated hydrocarbon such as cyclohexene was formed via dehydrochlorination. Ni catalysts used in

* To whom correspondence should be addressed.
E-mail: jyi@snu.ac.kr

1011-372X/03/0900–0185/0

the hydrodechlorination of chlorinated organic compounds were mostly supported on silica and zeolite, while very limited works for the hydrodechlorination of chlorinated organic compounds over Ni/Al_2O_3 catalysts have been reported [16,17].

Reported in this work are synthesis, characterization, and application of mesoporous γ-Al_2O_3 as a catalyst support for the hydrodechlorination of 1,2-dichloropropane (DCPA). Ni catalysts supported on mesoporous alumina were prepared by an impregnation (Ni-IMP) and vapor deposition (Ni-VD) method, and the effect of catalyst preparation method on the catalytic performance was examined. Physical and chemical properties of mesoporous alumina and supported Ni catalysts were characterized by nitrogen adsorption, small angle X-ray scattering (SAXS), transmission electron microscopy (TEM), powder X-ray diffraction (XRD), ultraviolet diffuse reflectance spectroscopy (UV-DRS), X-ray photoelectron spectroscopy (XPS), temperature-programmed reduction (TPR), and temperature-programmed desorption (TPD) of reactant (DCPA). To our knowledge, this is the first example reporting the hydrodechlorination over the Ni catalyst supported on mesoporous alumina.

2. Experimental

2.1. Synthesis of mesoporous alumina

Mesoporous alumina was prepared by a posthydrolysis method [7] at atmospheric pressure and at room temperature. 1.89 g of Al(sec-$BuO)_3$ (aluminum source) and 8.21 g of stearic acid (surfactant) were separately dissolved in 7.65 mL of sec-butyl alcohol, and the two solutions were then mixed. Some amounts of water were dropped into the mixture at a rate of 1 mL/min, until a white precipitate was formed. The resulting slurry was further stirred for 24 h, and subsequently, it was dried in air. The crude product was calcined at 450 °C for 3 h with a stream of air (50 mL/min). The temperature was raised up to 450 °C with a ramping rate of 1 °C/min, and maintained at 450 °C for 3 h to yield the final form.

2.2. Catalysts preparation

Powder of alumina support was pre-evacuated at 120 °C for 4 h to remove adsorbed water, and was followed by an air treatment at 200 °C to remove organic contaminants. Vapor deposition (VD) was performed in a stream of nitrogen using an organic complex of nickel acetylacetonate ($Ni(CH_3COCHCOCH_3)_2$ from TCI Co.) as a nickel precursor. The nickel precursor was gradually evaporated at 228 °C and adsorbed onto the surface of the alumina support. The resulting material was finally calcined at 450 °C with an airstream. ICP analysis showed that the composition of the supported Ni catalyst was 6.5 wt% Ni/Al_2O_3 (abbreviated as Ni-VD hereafter).

The supported Ni catalyst was also prepared by an impregnation method with an appropriate amount of aqueous solution of nickel nitrate. The prepared catalyst was dried overnight at 120 °C, and then it was finally calcined at 450 °C in air. Elemental analysis revealed that trace amounts of nitrogen (0.121%) and sulfur (0.025%) were included in the catalyst. It is expected that these impurities would show a negligible effect on the catalytic performance. ICP analysis showed that the composition of the resulting catalyst was 6.5 wt% Ni/Al_2O_3 (abbreviated as Ni-IMP hereafter).

2.3. Characterization

X-ray diffraction (XRD, M18XHF-SRA, MAC/Science) measurements were carried out in order to investigate the phase transformation of the synthesized alumina. Small angle X-ray scattering patterns were recorded on a GADDS (Bruker) using CuKα radiation to analyze periodicity. Adsorption isotherms of nitrogen were obtained with an ASAP-2010 (Micromeritics) apparatus. The pore size distribution was determined by the BJH method applied to the desorption branch of the N_2 isotherm. The size and location of Ni particles on the catalyst surface were confirmed by transmission electron microscopy (TEM, Joel, JXA-8900R) using an ultrasonically dispersed catalyst sample (in ethanol) deposited on a carbon grid. The metallic states of Ni species were confirmed by ultraviolet diffuse reflectance spectroscopy (UV-DRS, Perkin-Elmer, Ramda-20 spectrometer) within the range of 200–800 nm. The X-ray photoelectron spectra of the supported nickel catalysts were obtained with an AXIS-HS equipment. For the XPS measurements, the catalysts were calcined at 450 °C with an airstream. Calibration of binding energies of the $Ni2p_{3/2}$ emission line was done by using the C 1s line at 284.5 eV. The temperature-programmed reduction measurements were carried out in a conventional flow system with a moisture trap connected to a TCD at temperatures ranging from room temperature to 900 °C with a heating rate of 10 °C/min. For the TPR measurements, a mixed stream of H_2 (2 mL/min) and N_2 (20 mL/min) was used for 0.1 g of the catalyst sample. The catalysts reduced in the TPR apparatus under the same pretreatment conditions were examined once again by TPR measurements.

Temperature-programmed desorption profile of DCPA from each catalyst was determined in a conventional flow system equipped with a TCD. Prior to the TPD experiment, the catalysts were reduced with a stream of H_2 at 450 °C for 2 h, and then cooled down to the adsorption temperature of 100 °C with an inert gas stream. Gas-phase DCPA (4.58×10^{-2} mol) was fed to the catalyst for adsorption with a stream of N_2. The

physically adsorbed DCPA was removed by evacuation at the pressure of 2×10^{-2} torr. The sample was heated up to 100 °C, and maintained at this temperature for 1 h. Then the temperature was raised up to 700 °C with a ramping rate of 10 °C/min using N_2 (10 mL/min) as a carrier gas for 0.1 g of the catalyst sample.

2.4. Hydrodechlorination of 1,2-dichloropropane

Hydrodechlorination of 1,2-dichloropropane into propylene was carried out in a continuous flow fixed-bed reactor at an atmospheric pressure. Each catalyst (0.1 g) with a size of 150200 μm was charged into a tubular quartz reactor, and activated with a mixed stream of H_2 (20 mL/min) and N_2 (20 mL/min) at 450 °C for 2 h. The catalytic reaction temperature was maintained at 300 °C. DCPA (5.13×10^{-3} mol/h) was sufficiently vaporized by passing a preheating zone and fed into the reactor. The products were periodically sampled, and analyzed with a GC-MS and a gas chromatography (HP 5890 II, FID). The catalytic reactions were carried out several times for each catalyst under the same conditions. In each run, DCPA conversion and propylene selectivity were within the error range of ±5%.

3. Results and discussion

3.1. XRD and SAXS analyses

In order to investigate phase transformation and thermal stability of the synthesized alumina, XRD patterns were obtained as a function of calcination temperature. As shown in figure 1, as-synthesized alumina exhibits a mixed phase of bayerite and pseudoboehmite. γ-Al_2O_3 phase was formed at the calcination temperature of 270 °C, and this phase was still maintained at 450 °C. BET and FT-IR measurements (although these are not shown here) revealed that surface area and pore volume of γ-Al_2O_3 decreased drastically at the calcination temperature of 550 °C, demonstrating that γ-Al_2O_3 retained its stable structure up to 550 °C [7]. These results indicate that γ-Al_2O_3 obtained by the thermal treatment at 450 °C can serve as a stable support. In this work, therefore, Al_2O_3 sample was thermally treated at 450 °C to be used as a support for the Ni catalyst.

The SAXS patterns of mesoporous alumina and the supported Ni catalysts calcined at 450 °C are shown in figure 2. It is noteworthy that the SAXS patterns of mesoporous alumina and supported Ni catalysts exhibited a continuous decay without any peaks indicating the existence of a size-controlled porosity [18,19]. From these SAXS patterns, it can be inferred that the mesoporosity of these samples is much similar to the pore structure of HMS having randomly connected pore structure rather than that of MCM-41 or SBA-15 [18,19].

3.2. Nitrogen adsorption–desorption isotherms

Figure 3 shows the nitrogen adsorption–desorption isotherms measured for mesoporous alumina and supported Ni catalysts. The corresponding pore size distributions are shown in figure 4. As shown in figure 3, mesoporous alumina exhibits the IV-type isotherm and typical H2-type hysteresis loop. According to the literature [20], it was reported that a material showing H2-type hysteresis loop, which is common in many inorganic oxide gels, had interconnected network pore systems. On the other hand, a mesoporous silica such as SBA-15, a typical material showing H1-type hysteresis

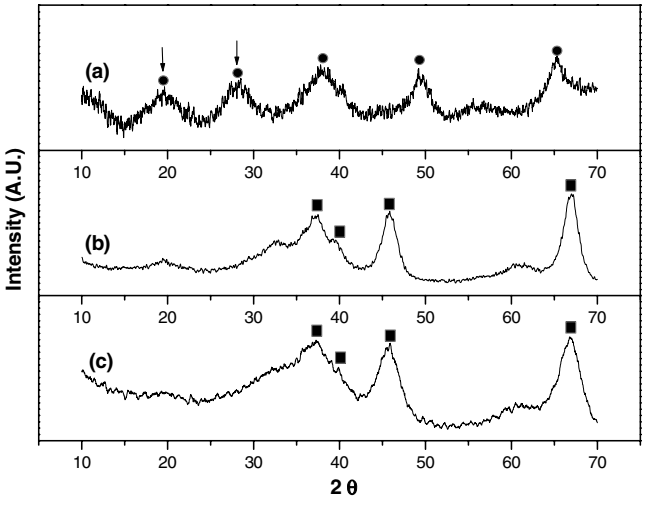

Figure 1. XRD patterns of alumina as a function of calcination temperature; (a) 25 °C (no treatment), (b) 270 °C, and (c) 450 °C; (●) bayerite, (↓) pseudoboehmite, (■) γ-Al_2O_3.

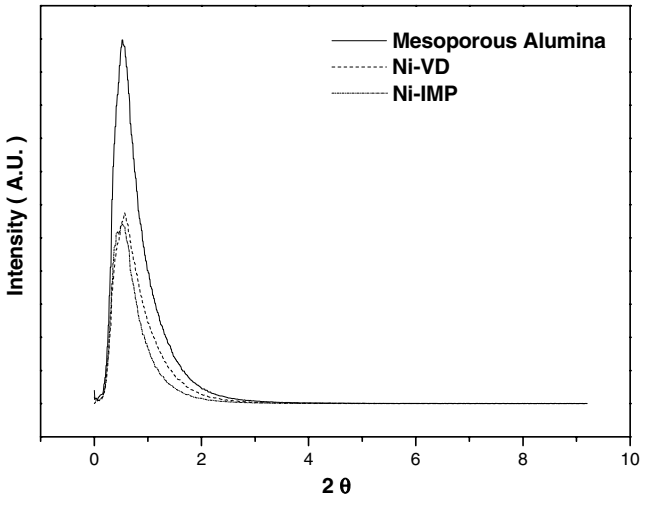

Figure 2. SAXS patterns of mesoporous alumina and supported Ni catalysts after calcination at 450 °C.

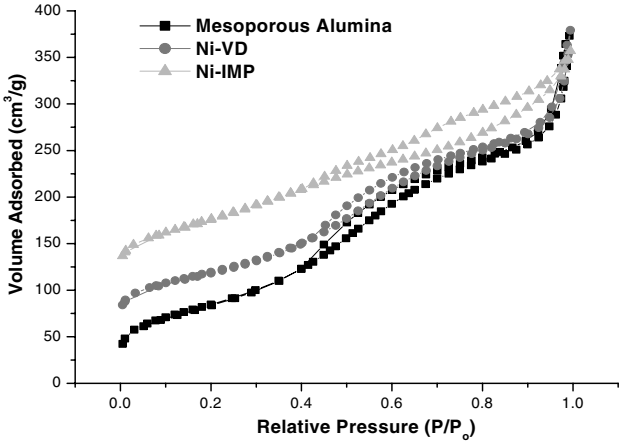

Figure 3. N_2 adsorption–desorption isotherms of mesoporous alumina and supported Ni catalysts after calcination at 450 °C.

loop, was reported to have regular pore array with uniform pore size distribution.

The Ni-VD catalyst shows similar shapes of isotherm and hysteresis loops to those of mesoporous alumina, while the features of the Ni-IMP catalyst are somewhat different from those of the mesoporous alumina. Figure 4 clearly shows that mesoporous alumina had very narrow pore size distributions centered at ca. 4 nm. The pore size distribution of the Ni-VD catalyst was nearly identical to that of the supporting material, although a slight shift toward small pore size was observed.

However, the Ni-IMP catalyst showed a different shape of pore size distribution from the other two samples. Two possible reasons can be considered for the modified pore characteristics of the Ni-IMP catalyst. One is the pore blocking after the impregnation. When metal precursors are impregnated on porous materials, especially on the support with large pore size, pore blocking by metals is inevitable. As shown in figure 3, however, the hysteresis loop of mesoporous alumina was changed from H2- to H3-type after impregnation of nickel precursor. As mentioned previously in the

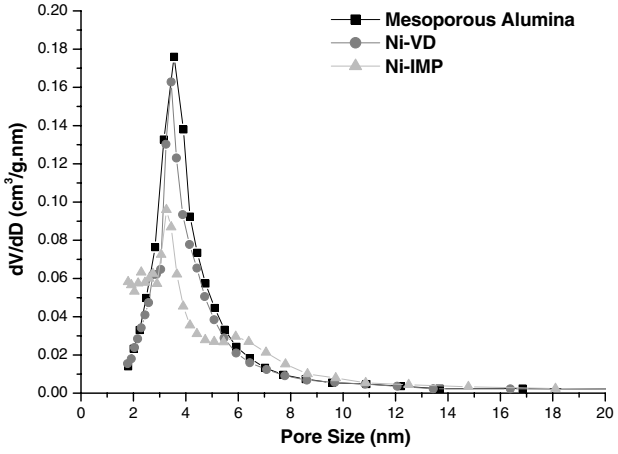

Figure 4. Pore size distributions of mesoporous alumina and supported Ni catalysts after calcination at 450 °C.

experimental section, the nickel loading was 6.5 wt%, a relatively small amounts of nickel. Therefore, it is inferred that pore blocking would not be a main reason. The other possibility affecting the pore size distribution of the Ni-IMP catalyst is the aluminum dissolution during the impregnation step. It is assumed that the pore walls of γ-Al_2O_3 were partly destroyed due to the aluminum dissolution in the impregnation step. Some researchers have reported aluminum dissolution from γ-Al_2O_3 in a nickel nitrate solution and acidic solution [21,22]. They observed that quite some amounts of aluminum ions were dissolved from alumina in a solution state, and the resulting alumina was reported to show the modified pore size distribution and adsorption isotherm. In our experiments, it is likely that aluminum ions were dissolved from the mesoporous alumina during the impregnation step for Ni-IMP preparation. In fact, it was observed that pH (measured with a Orion 960 pH meter) of the solution containing 6.5 wt% nickel precursor increased from 3.23 to 6.81 after addition of alumina into the solution. Although pore blocking can also be a possible reason for the modified pore characteristics of the Ni-IMP catalyst, it is believed that aluminum dissolution would be a main reason causing the modified pore size distribution and nitrogen adsorption–desorption isotherm of the Ni-IMP catalyst.

Surface area and pore volume of γ-Al_2O_3 and supported Ni catalysts are listed in table 1. Surface area and pore volume of the Ni-VD catalyst are somewhat larger than those of the Ni-IMP catalyst.

3.3. TEM and XPS analyses

Figure 5 shows the TEM images of mesoporous alumina and supported Ni catalysts reduced at 450 °C. TEM images of the reduced Ni catalysts showed the finely dispersed Ni particles, although some agglomerations larger than pore size were observed. No great difference in nickel particle size was observed between two catalysts.

In order to investigate the metallic state of Ni, XPS measurements for the calcined catalysts were carried out on the binding energy of Ni $2p_{3/2}$ level. As shown in figure 6, the band shapes and binding energies varied with respect to the catalyst preparation method. Compared to the XPS pattern of the Ni-VD catalyst,

Table 1
Surface areas and pore volumes of γ-Al_2O_3 support and Ni/γ-Al_2O_3 catalysts

Sample	Surface area ($m^2 g^1$)	Pore volume ($cm^3 g^1$)
γ-Al_2O_3	308	0.52
Ni-VD	271	0.39
Ni-IMP	254	0.32

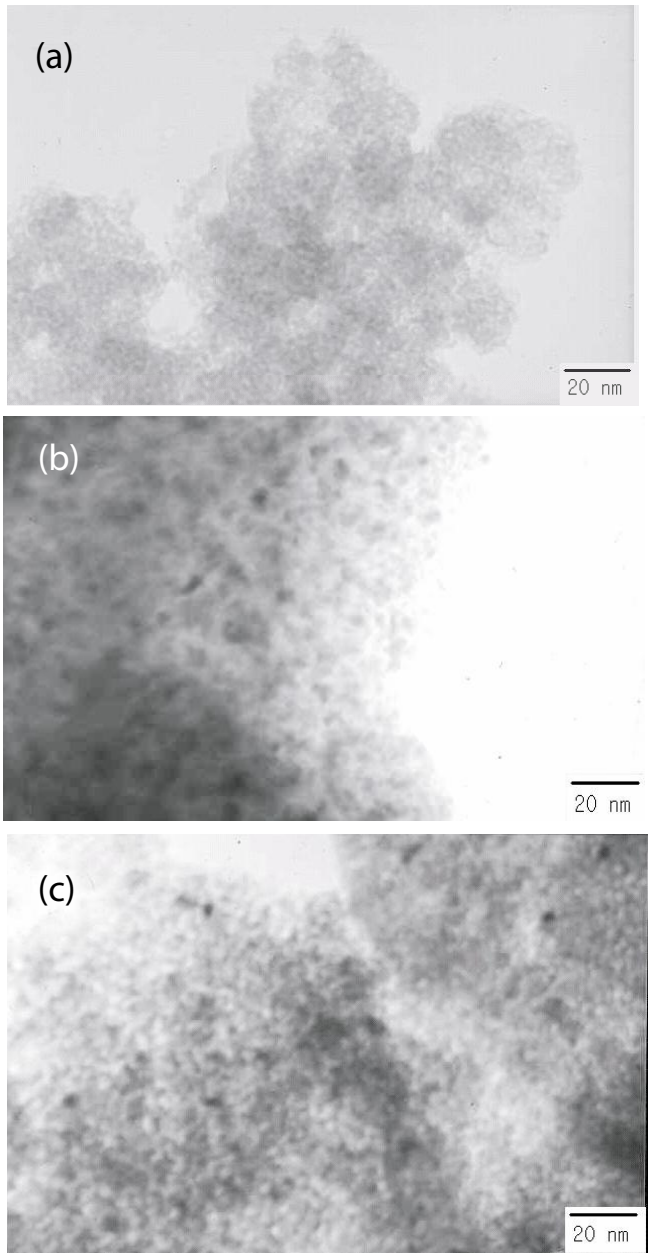

Figure 5. TEM images of (a) alumina support, (b) Ni-VD catalyst, and (c) Ni-IMP catalyst.

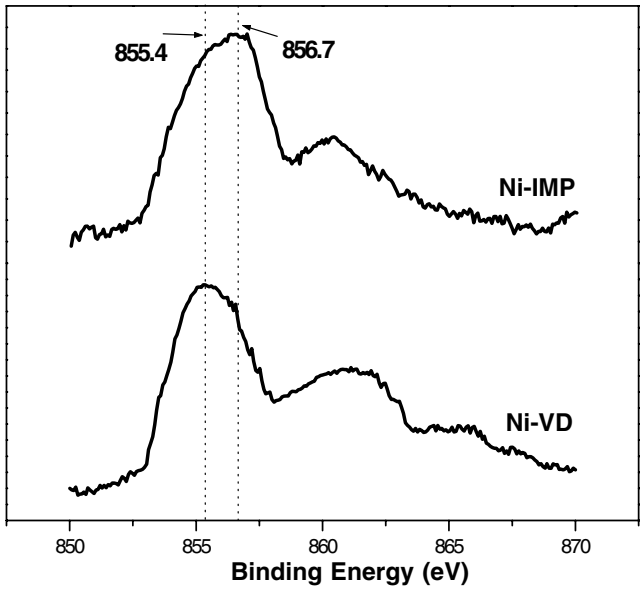

Figure 6. XPS spectra of supported Ni catalysts calcined at 450 °C with an airstream.

the Ni-IMP catalyst showed an asymmetric band shape and a shifted binding energy to higher value. The differences in band shape and binding energy between two samples strongly indicate the existence of different surface nickel species. It is known that the binding energy of pure NiO and Ni ion in the nickel aluminate are 855 eV and 857 eV respectively [23,24]. In this work, it was observed that the bandwidth of both catalysts was quite broad and the binding energies were slightly higher (855.4 eV for Ni-VD and 856.7 eV for Ni-IMP) than 855 eV, indicating different interaction between Ni species and mesoporous alumina. As shown in figure 6, it is noticeable that the binding energy contribution of nickel aluminate species in the Ni-IMP catalyst is much higher than that of the Ni-VD catalyst. This demonstrates that the Ni-IMP catalyst has large amounts of nickel aluminate species (which strongly interact with alumina) in its structure compared to the Ni-VD catalyst. On the other hand, NiO species (which weakly interact with alumina) are dominant in the Ni-VD catalyst.

3.4. TPR analyses

Figure 7 shows the TPR patterns of supported Ni catalysts. The reduction pattern of the Ni-IMP catalyst could be divided into three regions, while two reduction peaks were mainly observed in the Ni-VD catalyst. The low temperature reduction peak at around 400 °C, which can be assigned to some nickel aggregation, was observed in the Ni-IMP catalyst. It is noteworthy that the reduction peak above 800 °C, which can be attributed to the reduction of nickel aluminate-like species, is much stronger in the Ni-IMP catalyst than in the Ni-VD catalyst. As mentioned previously, this is presumably due to the aluminum dissolution that occurred during the nickel impregnation step. When nickel precursors are impregnated on alumina from a nickel nitrate solution, it is known that some parts of Al^{3+} located on the surface are dissolved into the solution by the hydrogen ions, and then the aluminum ions are competitively readsorbed on the surface together with the other ions such as nickel ions [25,26]. This mixed adsorption may cause the formation of some metal aluminate at the oxide surface [25]. Therefore, it is believed that the Ni-IMP catalyst retains considerable amounts of nickel aluminate species in its structure

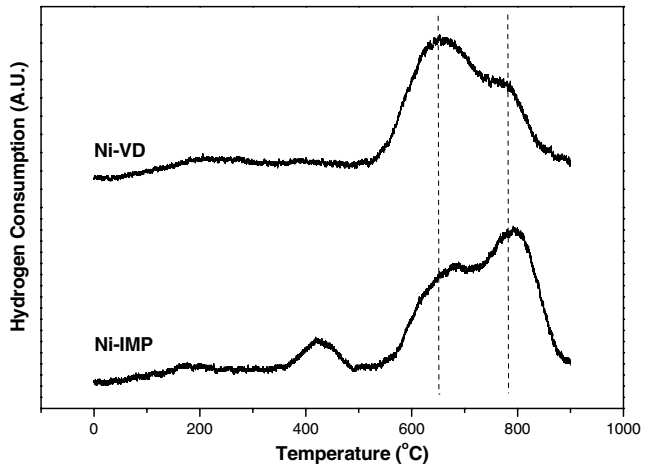

Figure 7. TPR patterns of supported Ni catalysts.

while the Ni-VD catalyst has low contents of nickel aluminate, as also evidenced from the XPS measurements.

3.5. UV-DRS analyses

In order to confirm the identity of nickel species and the formation of nickel aluminate, UV-DRS measurements for the supported Ni catalysts were taken as shown in figure 8. It was found that the colors of Ni-VD and Ni-IMP catalysts were different from each other. The latter was more greenish than the former. According to the literature [27], the color of nickel oxide is related to its electronic structure. The band at 715, 377, and/or 410 nm represents the octahedrally coordinated Ni^{2+} species in NiO lattices, while the band in the range of 600–645 nm represents the tetrahedrally coordinated Ni^{2+} species in nickel aluminate lattice. In the nickel aluminate spinel structure, it is well known that the ratio of octahedrally coordinated Ni^{2+} to tetrahedrally coordinated Ni^{2+} depends on the calcination temperature, calcination time, and ramping rate [28]. From this point of view, UV-DRS measurement can be a useful characterization technique for investigating the interaction between nickel and alumina support. Figure 8 shows that the Ni-IMP catalyst exhibits stronger intense of UV-DRS band at 600–645 nm than the Ni-VD catalyst, indicating that the phase of nickel aluminate spinel is much richer in the Ni-IMP catalyst than in the Ni-VD catalyst.

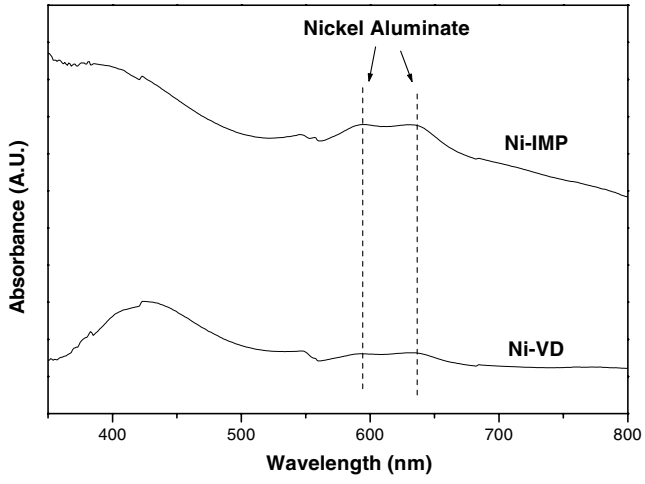

Figure 8. UV-DRS spectra of supported Ni catalysts.

3.6. Hydrodechlorination of 1,2-dichloropropane (DCPA)

Figure 9 shows the catalytic performance of supported Ni catalysts for the hydrodechlorination of 1,2-dichloropropane. In the catalytic reaction, propylene and chloropropylene were mainly produced, while trace amounts of ethylene and chloroethylene were detected by GC-MS. In previous works [11,15] investigating the gas-phase dechlorination of cyclohexyl chloride into cyclohexene, Tavoularis *et al.* reported that the direct formation of cyclohexene that occurred by the internal elimination of HCl, that is, via dehydrochlorination mechanism. The same authors investigating the effect of hydrogen partial pressure on the cyclohexene selectivity reported that the hydrogen partial pressure showed negligible effect on the yield of cyclohexene. While Choi *et al.* [13] pointed out in the hydrodechlorination of 1,2-dichloropropane that the chloropropylene selectivity depended on the hydrogen partial pressure and a certain level of hydrogen partial pressure was needed to maintain the constant level of propylene selectivity.

In our case, undoubtedly, chloropropylene would be a product of the dehydrochlorination, as suggested above by authors of references 11 and 15. From the point of view of authors of reference 13, however, it could not be fully understood if propylene was formed via dehydrochlorination mechanism. Therefore, further studies are still needed in order to elucidate the

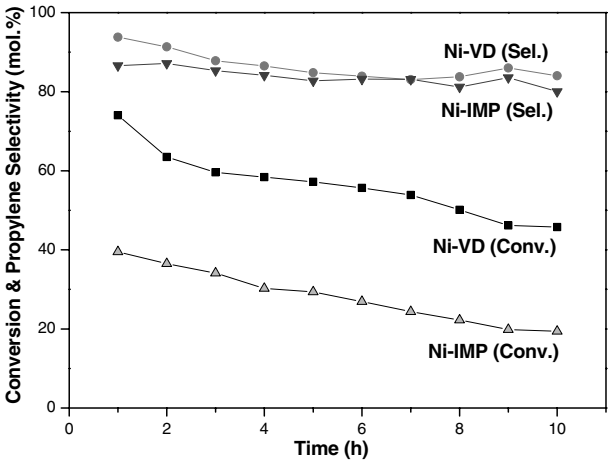

Figure 9. Conversion of 1,2-dichloropropane and propylene selectivity over supported Ni catalysts as a function of time on stream.

mechanism of propylene formation. In our catalytic reaction, in particular, any saturated hydrocarbons such as propane or chloropropane were not produced. This is because the activation energy for the hydrogenation of unsaturated hydrocarbon is higher than that for the cleavage of C–Cl bonding [13]. Another possible reason for the above result is that the adsorbed HCl on the catalyst surface inhibits hydrogenation ability of nickel, preventing further hydrogenation prior to the propylene desorption from the catalyst surface [11,15,29]. As shown in figure 9, propylene selectivities over both catalysts were slightly decreased at the initial stage of the reaction, and maintained at nearly constant level of ca. 83% or a little higher value. However, the supported catalysts exhibited great difference in DCPA conversions. DCPA conversion over the Ni-VD catalyst was about two times higher than that over the Ni-IMP catalyst.

This result can be explained with TPR (before and after reduction) and DCPA-TPD measurements. The TPR results are summarized in table 2. Clearly, the degree of reduction of the Ni-VD catalyst is much higher than that of Ni-IMP, indicating that the Ni-VD catalyst can be reduced more easily at the catalyst activation step than the Ni-IMP catalyst. Figure 10 shows the DCPA-TPD profiles of the supported Ni catalysts. The peak areas of DCPA-TPD profile (also summarized in table 2), an index of amounts of DCPA adsorbed on the catalyst, are closely related to the degree of reduction. At a first glance, it is clear that the Ni-VD catalyst adsorbs much more amounts of DCPA than the Ni-IMP catalyst. The particle size of active metal, of course, can also affect the amount of DCPA adsorption. However, TEM images showed no great difference in nickel particle size between two catalysts. Therefore, it is summarized that both the degree of reduction of nickel species and the amounts of adsorption of DCPA onto the catalyst are more closely related to the reducibility of the catalyst rather than the metal particle size. DCPA conversions could be directly correlated with the degree of reduction of nickel species and the amounts of adsorption of DCPA. In conclusion, the Ni-IMP catalyst containing large amounts of nickel aluminate spinels, which are more difficult to reduce into active nickel metals, exhibited lower catalytic performance than the Ni-VD catalyst. This means that relatively small portions of impregnated nickel particles in the Ni-IMP catalyst take part in the hydrodechlorination of 1,2-dichloropropane.

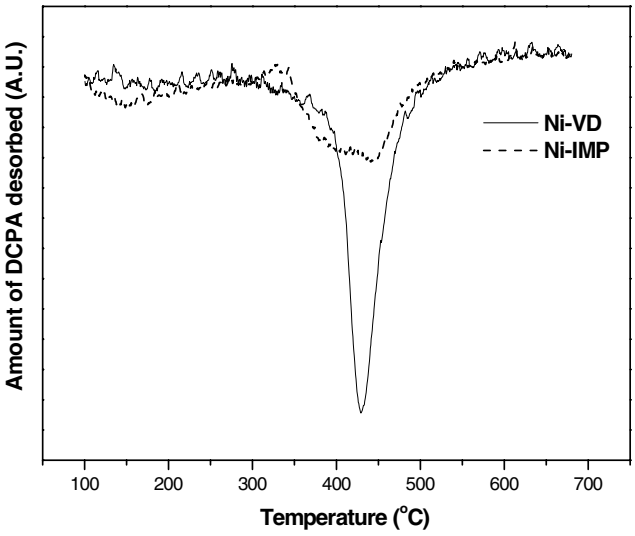

Figure 10. DCPA-TPD profiles of supported Ni catalysts.

4. Conclusions

A mesoporous alumina was successfully synthesized by a posthydrolysis method in this work. The mesoporous alumina was characterized to have relatively high surface area, sharp pore size distribution centered at ca. 4 nm, and randomly ordered pores. Ni catalysts supported on mesoporous γ-Al_2O_3 were prepared by a vapor deposition and impregnation method. It was observed that the Ni-VD catalyst maintained mesoporous pore structure, although surface area and pore size distribution was slightly shifted to lower values compared to the support, while the pore walls of the Ni-IMP catalyst were partly deformed by the aluminum dissolution that occurred during the impregnation step. From several characterizations, it was revealed that the aluminum dissolution that occurred in the preparation of the Ni-IMP catalyst caused the formation of nickel aluminate species, which are more difficult to reduce into active nickel metals than NiO. In the hydro-

Table 2
Analyses of peak area and area ratio of TPR (before and after reduction) and DCPA-TPD results

Catalyst	A_1 (A.U.)	A_2 (A.U.)	A_3 (%)	$A_{3Ni\text{-}VD}/A_{3Ni\text{-}IMP}$	A_4 (A.U.)	$A_{4Ni\text{-}VD}/A_{4NI\text{-}IMP}$
Ni-VD	70.77	53.26	24.7	1.74	98.66	1.60
Ni-IMP	71.17	61.03	14.2		61.80	

Note: A_1: peak area of TPR profile before reduction. A_2: peak area of TPR profile after reduction at 450 °C. A_3: defined as $(A_1 - A_2)/A_1$ (called the degree of reduction in this work). A_4: peak area of DCPA-TPD profile.

dechlorination of 1,2-dichloropropane, the Ni-VD catalyst, which has higher reducibility relative to the Ni-IMP catalyst, showed better catalytic performance.

Acknowledgments

This work was supported by the National Research Laboratory (NRL) program of the Korea Science and Engineering Foundation (KOSEF).

References

[1] C.T. Kresge, M.E. Leonowicz, W.J. Roth, J.C. Vartuli and J.S. Beck, Nature 359 (1992) 710.
[2] Y.S. Cho, J.C. Park, W.Y. Lee and J. Yi, Catal. Lett. 81 (2002) 89.
[3] Y. Park, T. Kang, Y.S. Cho, J.C. Park and J. Yi, Stud. Surf. Sci. Catal. (in press).
[4] Y. Kim, P. Kim, C. Kim, J.W. Choi and J. Yi, *Proc. 9th Asia-Pacific Conf. Chem. Eng*. (Christchurch, New Zealand, 2002) p. 86.
[5] Y. Liu, W. Zhang and T.J. Pinnavaia, Angew. Chem. Int. Ed. 40 (2001) 1255.
[6] Z. Zhang, Y. Han, L. Zhu, R. Wang, Y. Yu, S. Qiu, D. Zhao and F.S. Xiao, Angew. Chem. Int. Ed. 40 (2001) 1258.
[7] Y. Kim, B. Lee and J. Yi, Korean J. Chem. Eng. 19 (2002) 908.
[8] F. Vaudry, S. Khodabandeh and M.E. Davis, Chem. Mater. 8 (1996) 1451.
[9] S.B. Pu, J.B. Kim, M. Seno and T. Inui, Micro. Mater. 10 (1997) 25.
[10] S. Cabrera, J.E. Haskouri, J. Alamo, A. Beltran, S. Mendioroz, M.D. Marcos and P. Amoros, Adv. Mater. 11 (1999) 379.
[11] G. Tavoularis, M.A. Keane, J. Mol. Catal. A 141 (1999) 187.
[12] E.J. Shin, A. Spiller, G. Tavoularis and M.A. Keane, Phys. Chem. Chem. Phys. 1 (1999) 3174.
[13] Y.H. Choi and W.Y. Lee, Catal. Lett. 67 (2000) 155.
[14] Y.H. Choi and W.Y. Lee, J. Mol. Catal. A 174 (2001) 193.
[15] G. Tavoularis, M.A. Keane, Appl. Catal. A 182 (1999) 309.
[16] Y. Cesteros, P. Salagre, F. Medina and J.E. Sueiras, Appl. Catal. B 22 (1999) 135.
[17] A. Morato, L. Alonso, F. Medina, P. Salagre, J.E. Sueiras, R. Terrado and A. Giralt, Appl. Catal. B 23 (1999) 175.
[18] V. I. Parvulescu, H. Bonnemann, V. Parvulescu, U. Endruschat, A. Rufinska, W. Lehmann, B. Tesche and G. Poncelet, Appl. Catal., A 214 (2001) 273.
[19] W. Deng, P. Bodart, M. Pruski and B.H. Shanks, Micro. Meso. Mater. 52 (2002) 169.
[20] F. Rouguerol, J. Rouguerol and K. Sing, *Adsorption by Powders and Porous Solid; Principles, Methodology and Applications* (Academic Press, San Diego, 1999).
[21] S.L. Chen, H.L. Zhang, J. Hu, C. Contescu and J.A. Schwarz, Appl. Catal. 73 (1991) 289.
[22] J.A. Meith and J.A. Schwarz, Appl. Catal. 55 (1989) 137.
[23] P. Salage, J.L.G. Fierro, F. Medina and J.E. Sueiras, J. Mol. Catal., A 106 (1996) 125.
[24] M. Wu and D.M. Hercules, J. Phys. Chem. 83 (1979) 2003.
[25] R. Lamber and G. Schulz-Ekloff, J. Catal. 146 (1994) 601.
[26] B. Rebours, J.B. d'Espinose de la Caillerie and O. Clause, J. Am. Chem. Soc. 116 (1994) 1707.
[27] M.L. Jocomo, M. Schiavello and A. Cimino, J. Phys. Chem. 75 (1971) 1034.
[28] B. Vos, E. Poels and A. Bliek, J. Catal. 77 (2001) 198.
[29] E.J. Shin and M.A. Keane, Appl. Catal. B 18 (1998) 241.